

Snow microphysical observations in shallow mixed-phase and deep frontal Arctic cloud systems

H. Morrison,^{a*} P. Zuidema,^b G. M. McFarquhar,^c A. Bansemmer^a and A. J. Heymsfield^a

^aNational Center for Atmospheric Research, Boulder, Colorado, USA

^bRosentiel School of Marine and Atmospheric Science, University of Miami, Florida, USA

^cUniversity of Illinois, Urbana, Illinois, USA

*Correspondence to: H. Morrison, National Center for Atmospheric Research, 3450 Mitchell Lane, Boulder, 80301, United States. E-mail: morrison@ucar.edu

Snow particle size distributions (particle size $>400\ \mu\text{m}$) in the western Arctic measured with *in situ* aircraft instrumentation during the Surface Heat Budget of the Arctic/First ISCCP Regional Experiment - Arctic Clouds Experiment and Mixed-Phase Arctic Cloud Experiment are analysed. Three cases of shallow, precipitating mixed-phase boundary-layer clouds and two cases of deep, precipitating frontal clouds are examined. Overall, the shallow cases had much lower values of particle concentration and ice water content than the deep cases, indicating large differences in ice initiation and growth between these regimes. Within a given case for both the shallow and deep frontal systems, and for the dataset as a whole, crystal concentration had little correlation with temperature (height), despite an active aggregation process that was indicated by large aggregates ($>5\ \text{mm}$) observed in four out of the five cases. Exponential size distributions are fitted to the observations, allowing a direct comparison with the snow particle size distributions that are represented with exponential functions in many bulk microphysics schemes used in weather and climate models. Values of the fitted intercept parameter N_0 are generally 2–10 times smaller for the shallow compared to the deep frontal cases as a result of differences in crystal concentration between these regimes. Values of $N_0 \sim 10^7\ \text{m}^{-4}$ specified for snow in many bulk microphysics schemes are broadly consistent with fitted N_0 for the deep cases but larger than values for the shallow cases. The deep frontal cases also exhibit a relationship between N_0 and temperature consistent with previous observations of midlatitude frontal systems. However, there are no consistent differences in N_0 between the shallow and deep cases when partitioned by ice water content. Fitted values of slope parameter λ for the shallow and deep cases are generally consistent with previous studies of lower-latitude cloud systems. Copyright © 2011 Royal Meteorological Society

Key Words: microphysics

Received 7 July 2010; Revised 27 February 2011; Accepted 7 April 2011; Published online in Wiley Online Library 14 June 2011

Citation: Morrison H, Zuidema P, McFarquhar GM, Bansemmer A, Heymsfield AJ. 2011. Snow microphysical observations in shallow mixed-phase and deep frontal Arctic cloud systems. *Q. J. R. Meteorol. Soc.* **137**: 1589–1601. DOI:10.1002/qj.840

1. Introduction

Mixed-phase stratiform clouds occur frequently in the Arctic and are among the most radiatively influential cloud types (Shupe *et al.*, 2006). Despite their importance, these clouds tend to be poorly simulated by current climate

and weather models (Inoue *et al.*, 2006; Prenni *et al.*, 2007; Klein *et al.*, 2009; Morrison *et al.*, 2009a). Poor simulation is due in part to the representation of ice and snow microphysics (Jiang *et al.*, 2000; Morrison *et al.*, 2003; Prenni *et al.*, 2007; Luo *et al.*, 2008; Avramov and Harrington, 2010), including treatment of the snow particle

size distribution (PSD) (Morrison and Pinto, 2006; Solomon *et al.*, 2009).

Testing model microphysical representations for Arctic applications has traditionally been hampered by a lack of *in situ* Arctic data, but field experiments conducted within the last 10–20 years have begun to provide data with which to address this issue. While there have been several papers describing *in situ* ice microphysical observations gathered in the Arctic during these experiments (Pinto, 1998; Curry *et al.*, 2000; Lawson *et al.*, 2001; Gultepe *et al.*, 2004; Zuidema *et al.*, 2005; McFarquhar *et al.*, 2007; Verlinde *et al.*, 2007; Lawson and Zuidema, 2009), there has been relatively little testing of snow PSD parameter settings in microphysics schemes using these data. Furthermore, there has been limited comparison of ice and snow microphysical characteristics between different Arctic cloud types, or comparison with observations from lower-latitude systems, particularly midlatitude frontal clouds, which serve as the basis for parameter settings in many microphysics schemes.

Bulk microphysics parametrizations in weather and climate models generally assume an underlying functional form for the snow PSD. Many parametrizations assume exponential PSDs for the precipitating ice species (e.g. Lin *et al.*, 1983; Rutledge and Hobbs, 1983; Dudhia, 1989; Grabowski, 1998; Reisner *et al.*, 1998; Hong *et al.*, 2004; Thompson *et al.*, 2004; Morrison *et al.*, 2009b):

$$\frac{dN}{dD} = N_0 e^{-\lambda D} \quad (1)$$

where D is particle diameter, and N_0 and λ are the intercept and slope (inversely proportional to mean particle size) parameters of the PSD. The N_0 and λ parameters are related to ice particle number concentration N_i and ice (snow) water content IWC by (Morrison *et al.*, 2009b)

$$\lambda = \left\{ \frac{\Gamma(b+1)aN_i}{IWC} \right\}^{\frac{1}{b}}, \quad (2)$$

$$N_0 = N_i \lambda, \quad (3)$$

where Γ is the Euler gamma function and a and b are parameters in the power law mass–size (m – D) relationship $m = aD^b$, which are generally assumed to be constant over the PSD.

In most one-moment microphysics schemes, IWC (or snow mixing ratio) is predicted and N_0 is specified; λ is then derived from the predicted IWC and specified N_0 . A key point is that the specified values of N_0 in one-moment schemes are generally either constant (e.g. Lin *et al.*, 1983; Rutledge and Hobbs, 1983; Dudhia, 1989; Grabowski, 1998) or diagnosed as a function of IWC (Reisner *et al.*, 1998) or temperature T (Hong *et al.*, 2004; Thompson *et al.*, 2004) based on midlatitude observations and deep frontal clouds in particular (Gunn and Marshall, 1958; Sekhon and Srivastava, 1970; Houze *et al.*, 1979; Field *et al.*, 2005). Their application to Arctic clouds is therefore uncertain. Several microphysical process rates are dependent on snow N_0 , including vapour deposition/sublimation, riming and sedimentation, and studies have shown considerable sensitivity of model simulations to the specification of N_0 (Reisner *et al.*, 1998; Morrison and Pinto, 2006; Solomon *et al.*, 2009). Reducing N_0 by about an order of magnitude from values typically specified in bulk microphysics schemes led to substantially more realistic simulations of shallow

Arctic mixed-phase clouds (Morrison and Pinto, 2006; Solomon *et al.*, 2009). Thus, it is important to assess the realism of parametrizations by testing the specified values of snow N_0 against observations. However, up to this point there has been little evaluation of parametrized values of N_0 using *in situ* Arctic observations.

In this paper, we analyse ice and snow microphysical characteristics for two distinct and common Arctic cloud regimes: (i) shallow mixed-phase boundary-layer clouds with ice precipitation falling beneath the mixed-phase layer, and (ii) deep frontal clouds containing patches of supercooled liquid water embedded within deeper layers of ice that are more similar in terms of overall morphology to midlatitude frontal systems. Observations are synthesized by comparing and contrasting several different case-studies from two field experiments, with a focus on distributions of IWC , N_i and mass-weighted mean particle size, D_m . Exponential PSDs given by (i) are fitted to the observations and analysed. The emphasis is on differences in the fitted PSDs between the shallow and deep frontal regimes as well as comparison with lower-latitude observations and specified values of N_0 for snow in bulk microphysics schemes. It is important to test schemes with available datasets from the Arctic to characterize the appropriateness of the snow PSD parameter settings in models (specifically, N_0), even though these data are limited relative to many other regions. The findings presented herein, while based on a limited number of cases, can provide guidance for future studies using more comprehensive datasets as they become available.

The paper is organized as follows. Section 2 gives a description of the relevant instrumentation and measurements. A brief overview of each case is provided in section 3. Section 4 details the snow microphysical observations and analysis of IWC , N_i and D_m . Exponential PSDs are fitted to the observations and compared to the PSD representations in bulk microphysics schemes and lower-latitude observations in section 5. Conclusions are given in section 6.

2. Instrumentation and measurements

This study utilizes data gathered on several flights during the Mixed-Phase Arctic Cloud Experiment (MPACE: Verlinde *et al.*, 2007) and First ISCCP Regional Experiment - Arctic Cloud Experiment (FIRE-ACE: Curry *et al.*, 2000), which was co-ordinated with the Surface Heat Budget of the Arctic Ocean programme (SHEBA; Uttal *et al.*, 2002). There are a total of three flights from SHEBA/FIRE-ACE and MPACE analysed for the shallow cases, and two flights from SHEBA/FIRE-ACE for the deep frontal cases. Additional flights took place during MPACE and SHEBA/FIRE-ACE, but these cloud systems extended to mid-levels, were often multilayered, and were not clearly associated with any well-defined frontal passages. Hence these systems were not clearly distinguishable in either the shallow boundary layer or deep frontal regimes, and we leave analysis of these cases for future work. Additional cases were not included here because key instrumentation used in our analysis was either not included on the aircraft or was not working on these flights. The cases analysed here cover a range of synoptic conditions. The shallow cases occurred under weak synoptic-scale forcing with large-scale subsidence in the lower troposphere. The deep frontal cases had heavier precipitation associated with the approach and passing of the

synoptic-scale frontal systems. A more detailed description of the cases is given in section 3.

2.1. SHEBA/FIRE-ACE

SHEBA was focused on a heavily instrumented icebreaker ship frozen into the sea ice in the Beaufort Sea in autumn 1997 and allowed to drift with the pack ice for one year (Uttal *et al.*, 2002). During May and July 1998, the National Center for Atmospheric Research C-130 aircraft gathered measurements near the SHEBA site as part of FIRE-ACE (Curry *et al.*, 2000). Two-dimensional cloud (2D-C) and precipitation (2D-P) optical array probes were included on the C-130 for the FIRE-ACE/SHEBA (hereafter referred to as 'SHEBA') research flights. Their datasets were combined for the analysis here, with the breakpoint between the 2D-C and 2D-P particle size distributions set at 0.95 mm. The 2D-C has a 25 μm size resolution, with sizing and sample volume uncertain for sizes $<100 \mu\text{m}$ (Strapp *et al.*, 2001). The 2D-P probe nominally sizes particles up to 6.4 mm, but the effective sampling area has been increased to measure particles up to about 25 mm using an approach similar to Heymsfield and Parrish (1978). The Cloud Particle Imager (CPI) was also included on these flights and used for manual classification of particle habit and estimate of the phase (Lawson and Zuidema, 2009). Images from CPI for the three SHEBA cases (7 May and 26 and 28 July) have been archived at <http://cdp.ucar.edu/browse/browse.htm?uri=http://data.portal.ucar.edu/metadata/browse/arctic.thredds.xml> under the link 'SHEBA Ice Microphysical Images'. Additional instruments were included on the C-130 for measuring bulk liquid water mass content (King probe) and sizing of particles between 2 and 47 mm forward scattering spectrometer probe (FSSP-100). See Zuidema *et al.* (2005) and Lawson and Zuidema (2009) for a detailed discussion of the processing methods and measurement uncertainties associated with these instruments.

2.2. MPACE

MPACE took place during September and October 2004 and consisted of instrumentation at several ground sites in the North Slope of Alaska as well as flights in the vicinity of Barrow and Oliktok Point with the University of North Dakota Citation aircraft (Verlinde *et al.*, 2007). McFarquhar *et al.* (2007) describe the microphysical measurements from MPACE and associated processing techniques used here, except for the 2D-C as noted below. Instrumentation utilized for this study included the 2D-C, the High-Volume Precipitation Sampler (HVPS), and the CPI (the HVPS was not working on 9 October and the first flight on 10 October; hence, we do not include these cases in the analysis here). The HVPS nominally samples particles between 0.4 and 20 mm in size, with resolution of 0.3 to 1 mm, but undercounts for sizes smaller than about 800 μm (Heymsfield *et al.*, 2008). Similarly to the SHEBA dataset, particle size distributions have been generated from the combined 2D-C and HVPS data with the breakpoint set at 1 mm. Additional instrumentation on the Citation relevant to this study included a King probe, Particle Measuring Systems (PMS) Forward Scattering Spectrometer Probe (FSSP), and Counterflow Virtual Impactor (CVI: Twohey *et al.*, 2003; see McFarquhar *et al.* (2007) for a discussion of the specific CVI used during MPACE) which provided

bulk measures of total water content (*TWC*) greater than 1 mg m^{-3} .

2.3. Data

To minimize differences between the SHEBA and MPACE datasets, the 2D-C data for SHEBA and MPACE have been reprocessed using the same technique, which includes removing particles shattered on the instrument probe based on interarrival time following Field *et al.* (2006). The reduction in average total particle concentration ($D > 100 \mu\text{m}$) as a result of applying this correction ranges from $<1\%$ for the 7 May case to 16% on 26 July, with overall somewhat greater reduction for the deep compared to shallow cases. However, recent work directly comparing measurements from 2D-C with standard and modified protruding arms (with the modification designed to limit shattering) suggests shattered particles not removed by this correction could significantly enhance concentrations of particles smaller than about 400 μm , especially when the mean particle size is large (Korolev *et al.*, 2010). Thus, we focus the analysis on particles larger than 400 μm to avoid possible contamination by shattering.

Values of N_i are calculated by summing the differential number concentration (concentration per unit length) multiplied by the width of each bin from the 2D-C between 0.4 and 0.95–1 mm, and from the HVPS (MPACE cases) or 2D-P (SHEBA cases) for sizes larger than 0.95–1 mm. Calculations of *IWC* from the measured PSDs are difficult because ice particles are generally non-spherical and particle density is uncertain. Although measurements of *TWC* were made by the CVI during MPACE, in mixed-phase conditions the *IWC* could not be estimated as the difference between the CVI *TWC* and King liquid water content (*LWC*) because this represents a small difference of two large numbers (liquid typically dominates the mass of mixed-phase clouds), and hence has large fractional uncertainty (McFarquhar *et al.*, 2007). Instead, *IWC* is derived from the measured size distributions by

$$IWC = \sum_{j=1}^N N_j a D_j^b \Delta D_j \quad (4)$$

where N_j is the differential number concentration (concentration per unit length) in bin j , D_j is the mean size, and ΔD_j is the width of the bin in D -space, N is the total number of bins, and a and b are the parameters in the assumed power-law mass–size (m – D) relation that vary for different ice particle habits and sizes (e.g. Locatelli and Hobbs, 1974; Mitchell *et al.*, 1990). Here we use best-estimate a and b coefficients for each case, which are summarized in Table I. For the 10 and 12 October MPACE cases, we use the a and b coefficients from McFarquhar *et al.* (2007) that were derived from the MPACE dataset from 9 to 12 October by matching the *IWC* calculated following (4) with that directly measured by the CVI in all-ice conditions. For the 7 May SHEBA case, based on imaging from CPI, we choose a and b coefficients from Mitchell *et al.* (1990) for radiating assemblages of plates. These parameters were found to produce good agreement between millimetre-wavelength cloud radar (MMCR) reflectivity and that estimated from the *in situ* measured PSDs, relative to other m – D relations (Fridlind *et al.*, 2011). Finally, for the 26 and 28 July SHEBA

cases, the a and b coefficients are from Mitchell *et al.* (1990) for rimed dendrites, which were observed by CPI (although other habits were also observed), and also found to produce good agreement between the MMCR reflectivity and that estimated from the *in situ* PSDs relative to other m - D relations.

We emphasize that application of these m - D relations leads to uncertainty in the derived IWC , since it was not directly measured. The different m - D relations used here lead to a spread in the IWC of up to a factor of 5–6 for the largest IWC s. Other commonly-used m - D parameters for ice/snow particles, including those of Brown and Francis (1995), tend to lie within this range. A key point is that while this uncertainty should be kept in mind when interpreting the results, it does not affect the overall conclusions.

Here we assume that all particles larger than 400 μm are ice in subfreezing conditions. Large drops (D larger than a few hundred μm) were generally not discernible in imagery from the CPI at subfreezing temperatures for the SHEBA cases. McFarquhar *et al.* (2007) discuss in detail the particle phase for the MPACE flights in low-level mixed-phase clouds between 9 and 12 October. They analysed particle area ratio (projected area of the particle divided by the ratio of a circumscribed sphere) from CPI in mixed-phase conditions and found that only 10.6% of sampled particles larger than 125 μm had an area ratio larger than 0.8, corresponding with possible drizzle drops (this represents an upper limit since drizzle drops cannot be distinguished from quasi-spherical ice particles). Thus, while there is evidence for the occurrence of large supercooled liquid drops during the MPACE cases, they likely had very little contribution to total concentration of particles larger than 400 μm .

3. Case descriptions

This section gives an overview of the cases. Only a brief summary is provided here since the focus of this paper is on a synthesis of the ice microphysical observations and details of most of the cases have been described in previous papers.

3.1. Shallow boundary-layer clouds

The first three weeks of May over the SHEBA site ($\sim 76^\circ\text{N}$, 165°W) were dominated by a persistent low-level mixed-phase stratus. This case is described by Zuidema *et al.* (2005) and Fridlind *et al.* (2011). On 7 May the boundary layer (BL) was well-mixed from the surface to cloud-top, located at a height of about 600 m during midday and descending to 400 m by 0000 UTC 8 May (Figure 1(a)), with clear sky above. Note that the decrease of reflectivity below 0.2 km in Figure 1 is an artefact due to the MMCR 'dead zone' where the receiver is blanked to avoid damage to the electronics from the transmitted pulse. The SHEBA site was located under a broad ridge of high pressure extending across the Chuckchi and Beaufort Seas with large-scale subsidence at low levels. The upper portion of the cloud layer contained liquid (with maximum LWC of 0.07 g m^{-3}), as indicated from *in situ* observations and ground-based lidar depolarization measurements, with ice precipitation falling from the mixed-phase layer and reaching near the surface. IWC reached values of about 0.004 g m^{-3} , with $N_i < 0.5\text{ L}^{-1}$. Crystal habit determined from the CPI probe mostly consisted of single thick plates and side planes, which are the expected habit types for the conditions found in

this case with temperatures of -18 to -20°C and relative humidity near water saturation (Magono and Lee, 1966).

The 10 and 12 October MPACE cases consist of a single-layer, low-level mixed-phase stratocumulus cloud with ice precipitation falling from the mixed-phase layer to the surface (Figure 1(d)). These cases are described in detail by Verlinde *et al.* (2007) and McFarquhar *et al.* (2007). This cloud system formed as cold air was transported around a strong high-pressure centre north of Alaska from the pack ice edge over the relatively warm open ocean, resulting in large surface turbulent heat fluxes and formation of roll stratocumulus clouds. Aircraft sampled the clouds and precipitation between about 2100–2300 UTC on 10 October and 2300–2400 UTC on 12 October. The cloud top temperature was between about -13 and -16°C in the region sampled by the aircraft. While conditions were fairly steady during this period, there was a slight cooling of the lower troposphere. *In situ* measurements and lidar depolarization indicated a mixed-phase layer in the upper part of the boundary layer, with liquid water contents up to 0.3 to 0.4 g m^{-3} . These two MPACE cases have broadly similar microphysical characteristics, with IWC generally between 0.01 and 0.1 g m^{-3} and N_i up to 3 L^{-1} but generally less than 1 L^{-1} . CPI imaging suggests a mixture of particle habits throughout the depth of the cloud layer, including columns, irregulars and rosettes, as well as spheroids within the upper mixed-phase region (see Fig. 13 in McFarquhar *et al.* (2007)). Large (3–10 mm) irregular and rimed particles were also imaged by HVPS (see Fig. 10 in McFarquhar *et al.* (2007) for examples of individual HVPS, 2DC and CPI images).

3.2. Deep frontal systems

A low-pressure system to the northwest of SHEBA encouraged frontal passages over the ship ($\sim 79^\circ\text{N}$, 164°W) on both 26 and 28 July, and brought a relatively warm, moist, southerly flow over the SHEBA site prior to passage of the fronts. The case of 26 July was a classic frontal-type system with descending base of the hydrometeors (Figure 1(b)), upward large-scale vertical velocity, and decreasing surface pressure during the frontal approach. Precipitation began reaching the surface as rain at about 2300 UTC on 26 July, and continued until midday on 27 July. The C-130 aircraft sampled the clouds and precipitation in the vicinity of the SHEBA site from about 2030 UTC 26 July to 0300 UTC 27 July and between altitudes of 1.5 and 6.5 km. At subfreezing temperatures, IWC generally ranged between 0.05 and 0.5 g m^{-3} and N_i between 1 and 5 L^{-1} . Ice microphysical quantities had much less variability for this case than 28 July, consistent with the larger-scale ascent (with aircraft-observed vertical velocities generally less than 1 m s^{-1}) versus the more convective character of the frontal system on 28 July. Particle habits as imaged by CPI were varied, with bullet rosettes common above 5 km, sectored plates and dendrites at mid-levels, and columns, capped columns and heavily-rimmed dendritic crystals below 4 km (Figure 2). Supercooled liquid water was fairly limited and occurred in thin layers up to a height of 4.5 km, with LWC s up to 0.2 g m^{-3} at a temperature of about -10°C .

The 28 July case is described in detail by Lawson and Zuidema (2009; hereafter LZ09). This case is unique amongst cases observed during SHEBA, and perhaps all previous airborne studies conducted over the Arctic Ocean, because

Table I. Parameters in the mass–size (m – D) relationship $m = aD^b$ for each case (m in units of g, D in m).

Case	m – D relation	Reference
26 July	$m = 270.71D^{2.2}$	Mitchell <i>et al.</i> (1990), rimed dendrites
28 July	$m = 270.71D^{2.2}$	Mitchell <i>et al.</i> (1990), rimed dendrites
7 May	$m = 37.91D^{2.1}$	Mitchell <i>et al.</i> (1990), radiating assemblages of plates
10 October	$m = 1.696D^{1.7}$	McFarquhar <i>et al.</i> (2007)
12 October	$m = 1.696D^{1.7}$	McFarquhar <i>et al.</i> (2007)

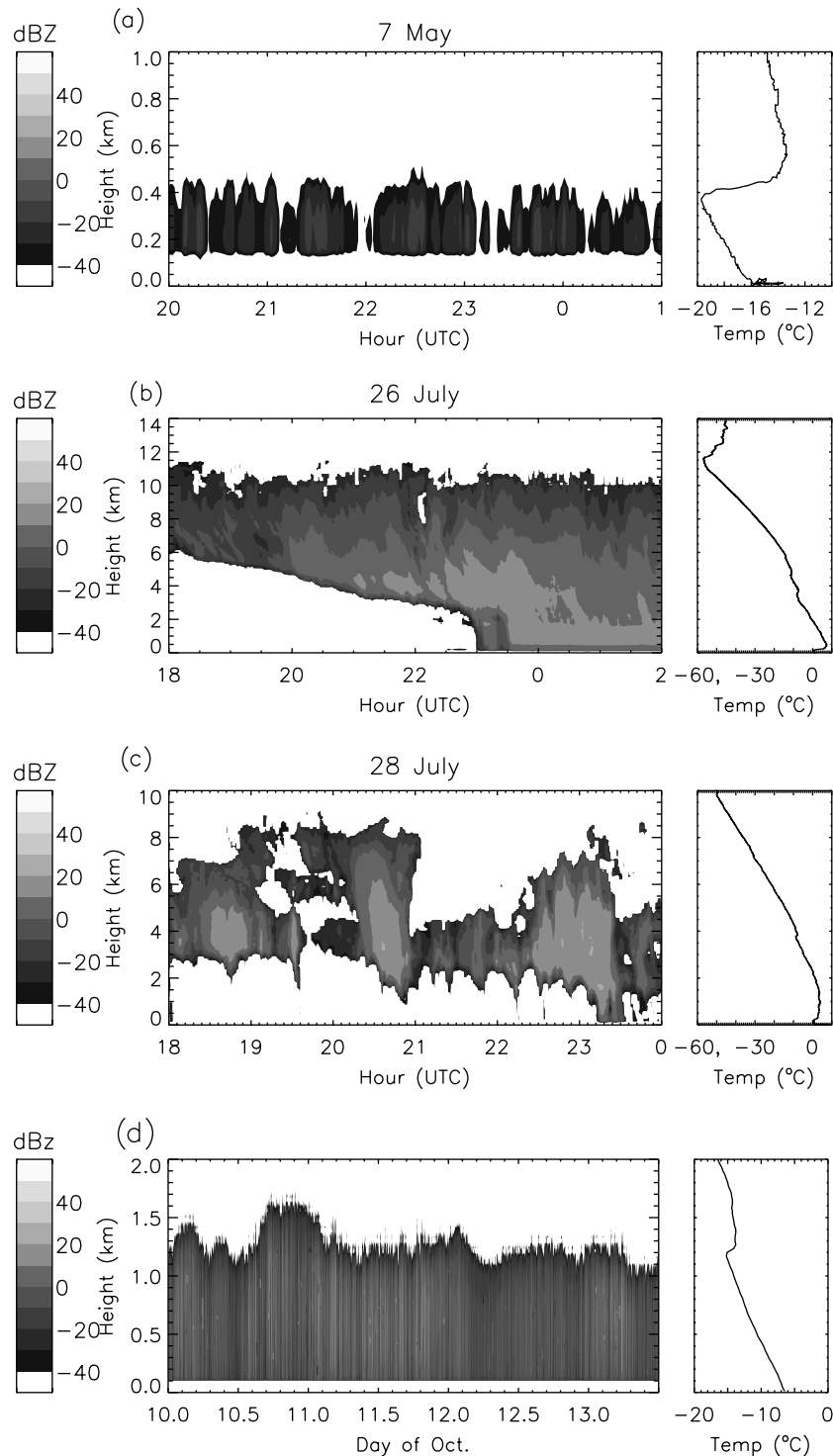


Figure 1. Time–height plots of MMCR reflectivity for the (a) 7 May, (b) 26 July and (c) 28 July SHEBA cases, and (d) 10–12 October MPACE cases. Also shown are temperature profiles from sondes launched at (a) 2335 UTC 7 May, (b) 2315 UTC 26 July and (c) 1900 UTC 28 July from SHEBA, and (d) 1101 UTC 11 October from Barrow, Alaska.

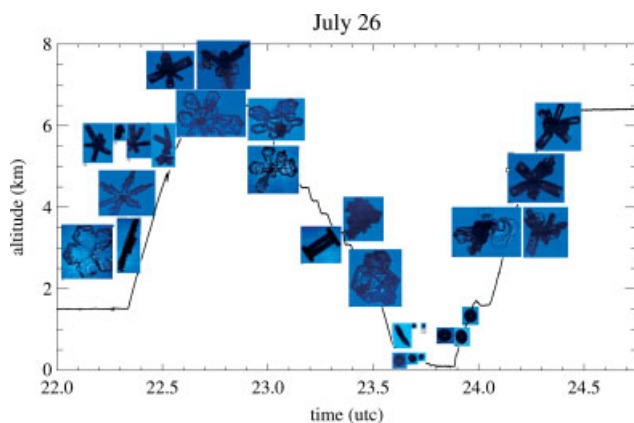


Figure 2. Sample images from CPI as a function of time and aircraft altitude in the vicinity of the SHEBA site on 26 July 1998.

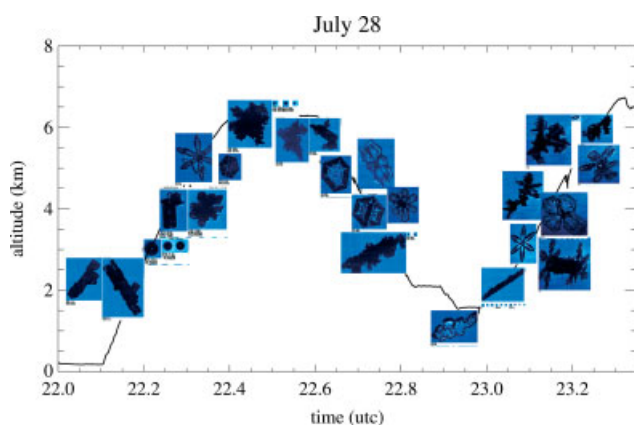


Figure 3. As in Figure 2, except on 28 July.

of embedded convection that produced graupel particles and 1 to 3 cm snowflakes. The base of the hydrometeors lowered during the day on 28 July, with precipitation for most of the day sublimating/evaporating as virga before reaching the surface (Figure 1(c)). Precipitation finally reached the surface after 2315 UTC, initially as rain. The aircraft sampled the cloud and precipitation at heights up to 6.4 km from about 2030 to 2330 UTC in the vicinity of the SHEBA site. Convective turrets with peak updraught velocities of 2 m s^{-1} had LWC s between 0.1 and 0.3 g m^{-3} , although supercooled liquid water was fairly limited overall. There was considerable variability in ice microphysical quantities associated with these turrets, with IWC up to 2 g m^{-3} and N_i up to 25 L^{-1} . Dendrites, plates, and sectored plates were common above 4 km, with columns and needles more common below 3 km (Figure 3). Many crystals were heavily rimed, even up to the highest flight level at $\sim 6 \text{ km}$.

4. Analysis of the ice microphysical data

In this section, we examine relationships between the various observed quantities and compare the shallow and deep frontal cases more generally. This analysis also provides context for the exponential PSDs fitted to the observations that are described in section 5. Scatterplots of IWC , T , N_i and D_m based on the 10 s data ($T < 0^\circ\text{C}$) and stratified between the deep frontal and shallow cases are shown in Figure 4. IWC , N_i and D_m are further analysed by averaging and binning the data into 5°C intervals. Mean values ± 1

standard deviation for each case are shown in Figure 5. Only points (10 s data) with calculated $IWC > 0.0001 \text{ g m}^{-3}$ are included in the averaging. Because of the long transit distance to reach the SHEBA site, only data obtained when the aircraft was in the vicinity of the SHEBA ship (defined as within a $1^\circ\text{lat} \times 5^\circ\text{long}$ cone surrounding the site) are used in the analysis for the SHEBA cases.

Overall, there is significant scatter among the cases. For the dataset as a whole, based on 10 s data, there is little correlation of N_i with T (correlation coefficient $r = -0.057$), D_m with N_i ($r = 0.177$), or IWC with T ($r = 0.198$). There is a weak positive correlation of D_m with T ($r = 0.511$), broadly consistent with the growth of particles as they fall. The lack of a stronger correlation of IWC or N_i with T reflects variability (horizontal and temporal) within a given case, as well as large variability between the cases. The shallow cases exhibit much lower values of IWC and N_i compared to the deep frontal cases, for the dataset as a whole but also at a given T . These results indicate substantial differences in crystal generation and growth between the shallow and deep regimes, which is not surprising given the large differences in dynamics and overall morphology. Low values of N_i for the shallow cases suggest relatively limited ice nucleation, which may be associated with depletion of ice nuclei locally in the Arctic boundary layer (Morrison *et al.*, 2005; Prenni *et al.*, 2007). Conversely, larger N_i for the deep cases may be associated with extension of the cloud top to cold temperatures more favourable for activation of ice nuclei (Fletcher, 1962; Pruppacher and Klett, 1997) as well as nucleation of ice over deeper layers, and subsequent settling of these crystals to lower levels. These results suggest that empirical relationships between microphysical quantities and local temperature may have limited usefulness because of the different generation and growth histories of particles observed at a given temperature for different cases and cloud regimes. These differences in N_i between the shallow and deep cases are broadly consistent with ice microphysical observations from 2D-C during the Complex Layered-Cloud Experiments (CLEX-5) described by Fleishauer *et al.* (2002). They found small N_i for shallow, mid-level clouds, with a mean of 0.7 L^{-1} , but values one to two orders of magnitude larger for a case of deeper cloud associated with an earlier frontal passage and embedded convection.

The use of different m - D relations for the shallow and deep cases (see Table 1) explains some of the differences in IWC , but mean IWC s still generally differ by an order of magnitude or more between the shallow and deep cases using the same m - D relation for all cases. There are no substantial differences in D_m between the shallow and deep clouds; thus, much of the difference in IWC between the shallow and deep cases is explained by the lower values of N_i , rather than D_m . There is a weak positive correlation of D_m with IWC for the dataset as a whole ($r = 0.491$) based on the 10 s data (Figure 4(e)). A stronger relationship exists between N_i and IWC ($r = 0.759$), with the best-fit line given by $N_i = 5.33IWC^{0.627}$ (N_i in units of L^{-1} and IWC in units of g m^{-3}) (Figure 4(d)). This best-fit curve (as well as those described in section 5) is calculated using the bivariate method of York *et al.* (2004), with equal weighting given to all data points. There is also strong correlation between N_i and IWC for the individual cases.

While the shallow cases in general have much smaller IWC and N_i than the deep frontal cases, there is substantial

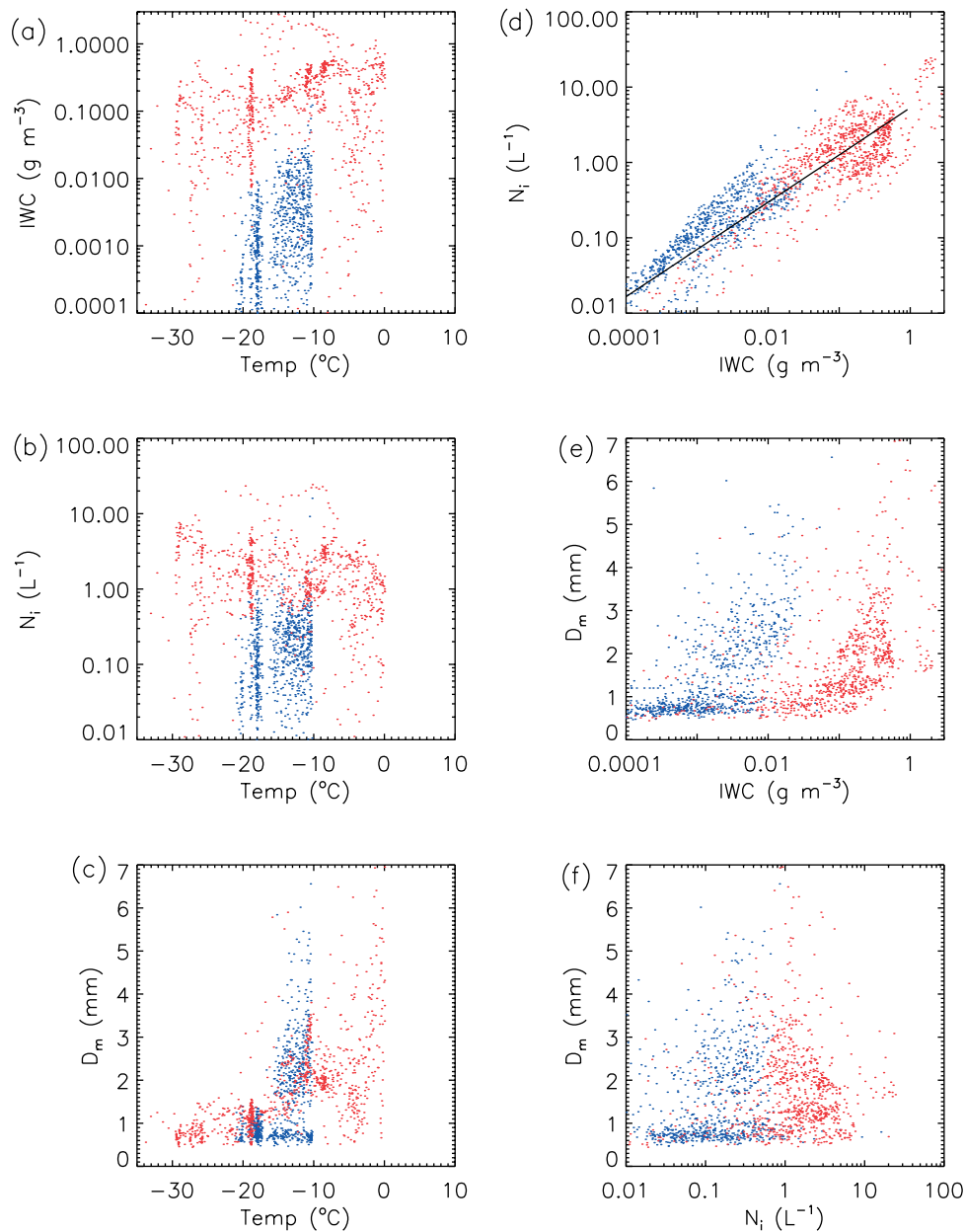


Figure 4. Scatterplots of (a) T and IWC , (b) T and N_i , (c) T and D_m , (d) IWC and N_i , (e) IWC and D_m , and (f) N_i and D_m . Shown are 10 s data, with blue indicating shallow cases (10 and 12 October and 7 May) and red indicating deep frontal cases (26 and 28 July). The solid line indicates the best-fit curve for the $IWC-N_i$ relationship (see text for details).

variability amongst these cases. The 10 and 12 October cases, not surprisingly, have fairly similar microphysical characteristics, while 7 May has mean IWC and N_i that are 5–10 times smaller. Using 10 s data and combining all of the shallow cases, there are weak positive correlations between T and IWC ($r = 0.299$), Z_c (vertical distance from cloud top) and IWC ($r = 0.222$), and Z_c and D_m ($r = 0.376$). However, these correlations are weaker when calculated for individual cases. Poor correlation of IWC and D_m with Z_c within a given case reflects significant horizontal variability, as well as vertical mixing as described in more detail below. There is little correlation of N_i with T considering all of the shallow cases together ($r = 0.124$) or individually.

The presence of large aggregates (3–10 mm) for the MPACE cases, as ascertained from the HVPS probe, is consistent with broad particle size spectra (Figure 6). There is an increase in the concentration of particles larger than 1 mm with increasing temperature (decreasing height) as seen in

the spectra on 10 October, which is consistent with growth by aggregation. However, the presence of large particles throughout the depth of the cloud layer in these cases, even near cloud top, suggests the role of turbulence in mixing particles throughout the cloud layer. This is consistent with vertical velocities of about $\pm 1 \text{ m s}^{-1}$ within the BL as measured by the aircraft. The role of turbulence and mixing on ice PSDs was also evident in shallow mixed-phase cloud systems observed during the recent (spring 2008) Indirect and Semi-Direct Aerosol Campaign (ISDAC: McFarquhar *et al.*, 2010). Vertical mixing, in addition to horizontal variability, may also help to explain the lack of strong correlation between D_m and Z_c for these cases, despite the growth of ice particles by vapour diffusion and riming as they fell through this environment. In contrast to the MPACE cases, the size spectra on 7 May are much narrower (Figure 6), with almost no particles larger than 3 mm and very little increase in the concentration of large particles with

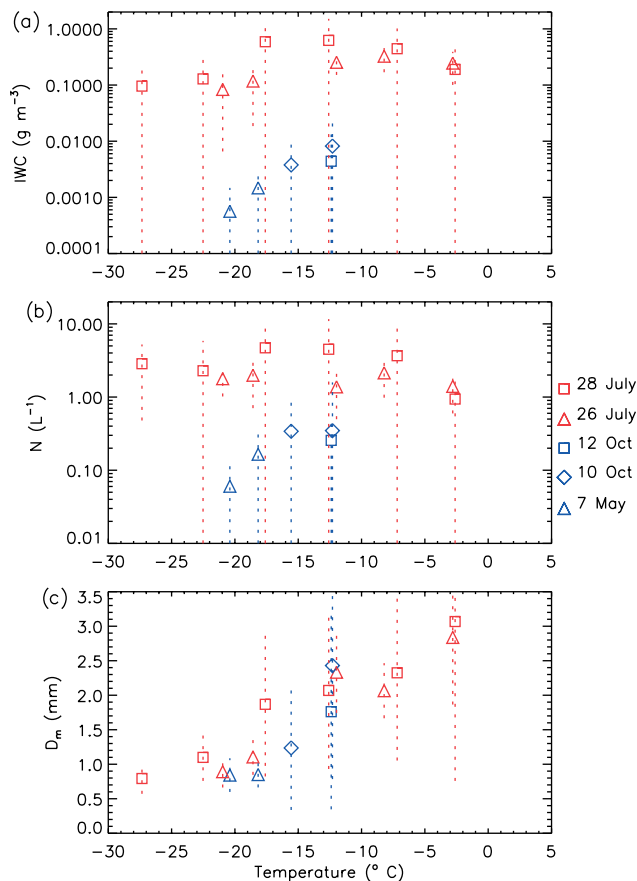


Figure 5. (a) IWC , (b) N_i and (c) D_m as a function of temperature. Case-average values are shown by the symbols, with the vertical dotted line indicating ± 1 standard deviation based on 10 s data.

increasing T . These results, in addition to particle imaging, indicate that aggregation was limited for this case. Low values of N_i and the shallow cloud depth likely contributed to the lack of aggregation, as well as crystal habits consisting mostly of thick plates and side planes which have a low aggregation efficiency (Pruppacher and Klett, 1997). Sublimation had limited impact on the shallow cases, given that the BL was ice supersaturated over all but the lowest few hundred metres.

Ice microphysical characteristics are fairly similar for the two deep frontal cases, despite substantial differences in the dynamics. However, the convective nature of the 28 July case is consistent with much more horizontal variability of the microphysical quantities compared to 26 July. Overall, correlation of IWC with T is weakly positive ($r = 0.193$) for these two cases ($T < 0^\circ\text{C}$). A decrease of IWC at temperatures above -5°C on both 26 and 28 July (Figure 5(a)), which occurred near the base of the cloud/precipitation, is indicative of sublimation. While particle imaging indicated the existence of large aggregates on both 26 and 28 July, there is no clear decrease of N_i with increasing temperature or decreasing height (correlation of N_i with T is very weakly negative with $r = -0.109$ using the 10 s data for these cases, see Figure 4(c)), as would be expected if aggregation were the dominant process controlling the vertical distribution of N_i . It is likely that horizontal variability, especially on 28 July, contributed to the lack of correlation between N_i and T .

Another possible explanation for the relatively constant N_i with temperature (and height), despite an active aggregation process, is new particle formation (primary

and/or secondary) lower in the cloud layer that may have helped to balance the depletion of N_i through aggregation. This hypothesis is consistent with particle size spectra at various levels shown in Figure 7. There is a general increase in the concentration of large particles ($D > 1$ mm) with increasing T (decreasing height), indicating growth by diffusion, riming and aggregation, and consistent with the large single crystals and aggregates that were imaged at lower levels. However, there is not a corresponding decrease in the concentration of particles smaller than 1 mm, except on 28 July at temperatures between -5 and 0°C . This signature of enhanced aggregation on 28 July at the warmest temperatures is also suggested by the rapid increase of D_m near 0°C to values that exceed 5 mm as seen in Figure 4(c). This may be related to enhanced aggregation efficiencies due to formation of an ice bond across the surface of contact between the aggregating particles at temperatures near freezing (Pruppacher and Klett, 1997).

Based on the available measurements, we cannot confirm nor rule out specific mechanisms that may have led to ice particle formation lower in the cloud system such as collisional breakup (e.g. Vardiman, 1978) or primary nucleation associated with droplet freezing and/or evaporation (e.g. Fridlind *et al.*, 2007). Columnar and needle crystals were imaged by CPI at low levels on both 26 and 28 July (see Figures 2 and 3), which is consistent with the initiation and growth of particles in conditions supporting rime splintering ($-8 < T < -3^\circ\text{C}$) according to Hallet and Mossop (1976), but there is not a noticeable increase in particle concentration in locations with these conditions. Thus, there is some observational support for rime splintering but its importance for these cases is uncertain.

5. PSD parameter fits and implications for modelling

In this section, we fit complete exponential functions given by (1) to the observed snow PSDs to derive N_0 and λ . We note that while some average spectra are well-described by exponential functions (e.g. 7 May, see Figure 6), individual PSDs (i.e. based on 10 s averages) often deviate from the exponential form. Despite these deviations, we fit the observed PSDs to exponential functions to allow for a direct comparison with the snow PSDs represented in most bulk microphysics schemes.

Fitted PSDs are calculated for each 10 s data segment with $IWC > 0.0001$ g m $^{-3}$ and $T < 0^\circ\text{C}$. We employ a moment-fitting technique similar to Heymsfield *et al.* (2008) to derive N_0 and λ for each of the PSDs. These parameters are derived using fits to the N_i and IWC assuming a threshold size $D_{th} = 400$ μm , which is consistent with the N_i and IWC discussed in section 4 and avoids potential issues with enhanced small particle concentrations from shattering on the 2-DC that were not removed by the Field *et al.* (2006) algorithm (see section 2.3). We also calculate case-average fitted PSDs using an approach similar to McFarquhar and Black (2004), whereby average size distributions are generated by stratifying data from each flight into different ranges of IWC and T . For temperature, data are binned every 5 K. For IWC , data are binned within the intervals of 0.0001, 0.001, 0.01, 0.05, 0.1, 0.5 and >0.5 g m $^{-3}$. Average spectra were only calculated for T and IWC bins for which there were at least 30 s of data.

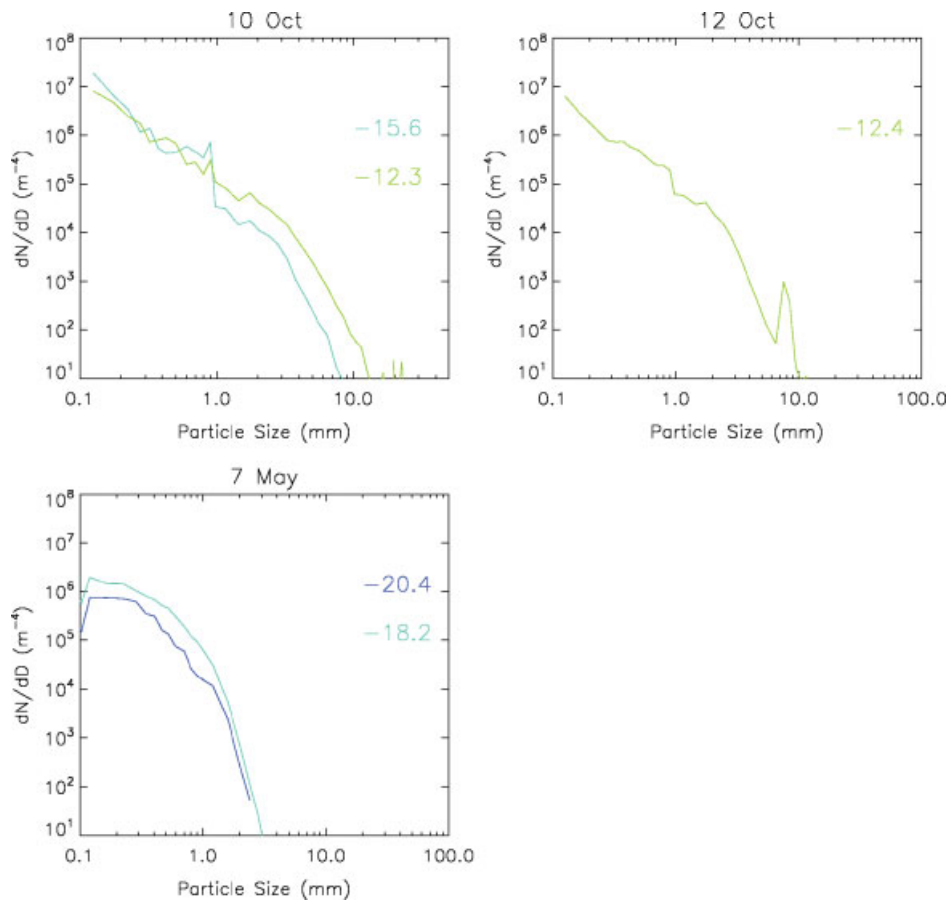


Figure 6. Particle size spectra for the shallow cases (10 and 12 October and 7 May) averaged and binned over 5°C temperature intervals. Only 10 s data with IWC exceeding 0.0001 g m^{-3} is used in the averaging. Mean temperature ($^{\circ}\text{C}$) of each interval is indicated in the plots.

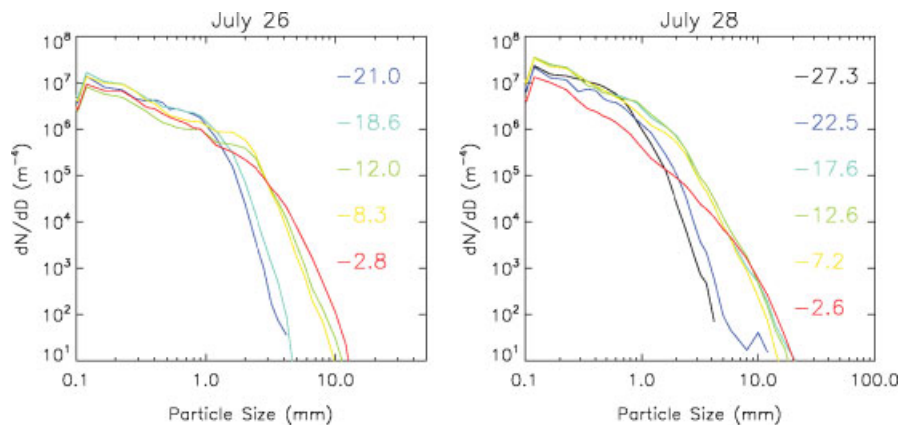


Figure 7. As in Figure 6 except for the deep frontal cases (26 and 28 July).

Plots of N_0 from the 10 s and case-average fitted PSDs as a function of IWC and T are shown in Figure 8. There is considerable scatter of N_0 among the cases. The shallow cases have values of N_0 generally 2 to 10 times smaller than in the deep frontal cases overall and for a given T . Small values of N_0 for the shallow cases result from the much smaller values of N_i compared to the deep cases, presumably due to differences in ice particle initiation between these regimes as discussed in section 4. While there is little correlation between N_0 and T for the dataset as a whole, values of N_0 tend to decrease with increasing T for the deep frontal cases, which is consistent with observations in midlatitude frontal systems (Houze *et al.*, 1979; Field *et al.*, 2005) that have served as the basis for parametrization of snow N_0 as

a function of T in some microphysics schemes (e.g. Hong *et al.*, 2004; Thompson *et al.*, 2004). When partitioned by IWC there are no consistent differences in N_0 between the shallow and deep cases, although the IWCs in the shallow cases are generally restricted to values less than 0.02 g m^{-3} while the deep cases have larger IWCs. One-moment schemes that specify constant N_0 with values between 8×10^6 to $2 \times 10^7\text{ m}^{-4}$ (Rutledge and Hobbs, 1983; Dudhia, 1989; Grabowski, 1998) are more consistent with the deep frontal cases, and generally larger than in the shallow cases. Conversely, the constant N_0 of $3 \times 10^6\text{ m}^{-4}$ in the Lin *et al.* (1983) scheme is more consistent with the shallow cases, but smaller than in the deep frontal cases.

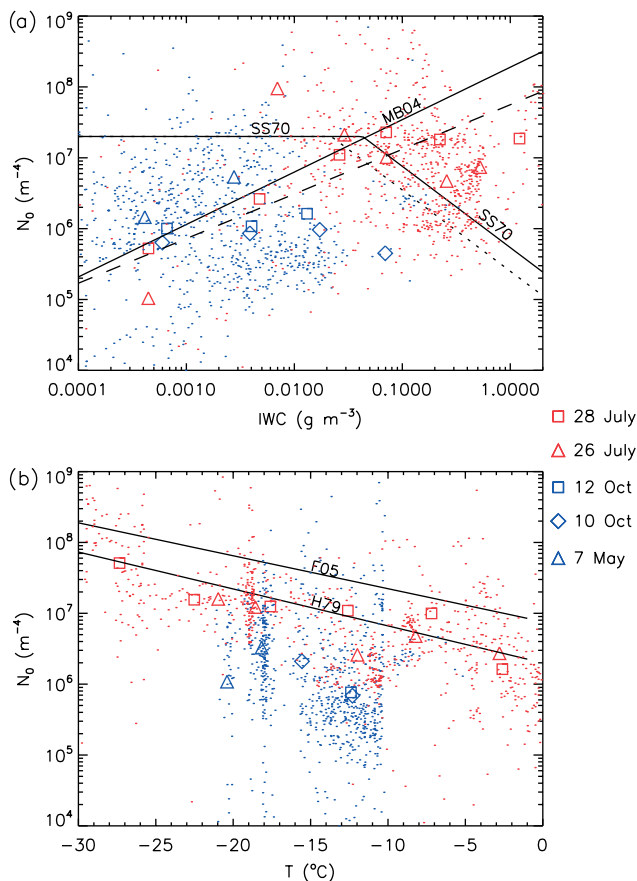


Figure 8. Fitted N_0 using $D_{\text{th}} = 400 \mu\text{m}$ as a function of (a) ice water content, IWC , and (b) temperature, T , for the 10 s data (dots) and case-average spectra (symbols). Results for the shallow and deep cases are shown in blue and red, respectively. Also shown are the relationships from Sekhon and Srivastava (1970; SS70) as implemented by Reisner *et al.* (1998), McFarquhar and Black (2004; MB04), Field *et al.* (2005, F05), and Houze *et al.* (1979; H79). The dotted line shows the SS70 relationship with a correction to account for inconsistencies in the melted versus unmelted particle size. The dashed line indicates best-fit N_0 - IWC relationship (see text for details).

There is an overall increase of N_0 with IWC for the dataset as a whole, albeit with significant scatter (Figure 8(a)). The best-fit curve for this relationship (based on the 10 s data) is given by $N_0 = 5.62 \times 10^7 IWC^{0.630}$ ($r = 0.337$; N_0 in units of m^{-4} and IWC in g m^{-3}). Following (2) and (3), if N_i increases with IWC at a rate greater than $IWC^{\frac{1}{b+1}}$, then N_0 increases with IWC . Conversely, if the rate of increase of N_i with IWC is smaller, then N_0 decreases with IWC . Previous observational studies of lower-latitude clouds have widely disagreed on the relationship between N_0 and IWC . The N_0 - IWC relationship implemented in the Reisner *et al.* (1998) microphysics scheme, based on midlatitude observations of Sekhon and Srivastava (1970; hereafter SS70), shows a decrease of N_0 with increasing IWC , for IWC greater than about 0.03 g m^{-3} (we also show this relationship using a correction for inconsistencies in the melted versus unmelted particle size between the original relationship proposed by SS70 and that implemented by Reisner *et al.* (1998)). Heymsfield *et al.* (2008) also show a decrease of N_0 with IWC for subtropical, convectively generated clouds. In contrast, the N_0 - IWC relationship of McFarquhar and Black (2004), based on aircraft observations taken in tropical cyclones, suggests an increase of N_0 with IWC somewhat more consistent with the results here. However,

the McFarquhar and Black (2004) relationship exhibits a steeper increase of N_0 with IWC .

Plots of λ as a function of IWC and T for the 10 s and case-average fitted PSDs are shown in Figure 9. For a given IWC , values of λ tend to be smaller for the shallow compared to the deep frontal cases. There is a decrease of λ with IWC which reflects the direct relationship between these variables as expressed in (4). The best-fit line for this relationship (based on the 10 s data) is given by $\lambda = 1380 IWC^{-0.147}$ ($r = -0.472$; λ in units of m^{-1} and IWC in g m^{-3}). These results are consistent with SS70, although the slope of their relationship is more negative (here we have converted the λ -precipitation rate relationship from SS70 to a λ - IWC relationship following the approach used by Reisner *et al.* (1998)). This relationship has also been modified to account for inconsistencies in the melted versus unmelted particle sizes between the original observations of SS70 and the approach of Reisner *et al.* (1998). The shallow cases exhibit somewhat larger values of λ than the deep cases for a given IWC , which is consistent with smaller values of D_m as a function of IWC for the shallow cases (see Figure 4(e)).

The fitted PSDs binned according to T suggest that λ decreases with increasing temperature (Figure 9(b)), which is consistent with the increase of mean size D_m with T and growth of particles through the depth of the cloud layer as discussed in the previous section. Previous studies have also suggested an inverse relationship between λ and T in mid- and lower-latitude clouds (Houze *et al.*, 1979; Ryan, 2000; Heymsfield, 2003). The λ - T relationships derived from these earlier studies are in close agreement with one another and are similar to the results shown here.

Most bulk microphysics schemes separate ice into different species to represent small ice particles (cloud ice) and larger ice and/or aggregates (snow). Separation between cloud ice and snow is fairly arbitrary and different schemes use different approaches. Here we assume that all observed particles larger than $D_{\text{th}} = 400 \mu\text{m}$ correspond to the snow category, but this may be inconsistent with the partitioning between cloud ice and snow in some bulk microphysics schemes. To explore this issue, we recalculated the fitted PSDs using different values of D_{th} (not shown). Values of N_0 and λ change with an increase of D_{th} to $800 \mu\text{m}$ or decrease to $100 \mu\text{m}$, but there is little impact on the overall results. Namely, for all values of D_{th} used here there is an increase of N_0 with IWC for the dataset as a whole, little correlation of N_0 with T , and values of N_0 about 2 to 10 times smaller for the shallow compared to the deep cases overall and for a given T . There is a tendency for increased scatter and reduced correlation of the fitted PSD parameters with T or IWC as D_{th} is increased. Results using $D_{\text{th}} = 100 \mu\text{m}$ are similar to those using $D_{\text{th}} = 400$ or $800 \mu\text{m}$, despite the possible impact of enhanced concentrations of particles smaller than $400 \mu\text{m}$ due to shattering on instrument probes.

6. Summary and conclusions

This study analysed ice particle size distributions ($D > 400 \mu\text{m}$) measured with *in situ* aircraft instrumentation for two distinct cloud regimes observed during the SHEBA/FIRE-ACE and MPACE field experiments in the western Arctic. Three cases of shallow, precipitating mixed-phase boundary-layer clouds and two cases of deep, precipitating frontal clouds were analysed.

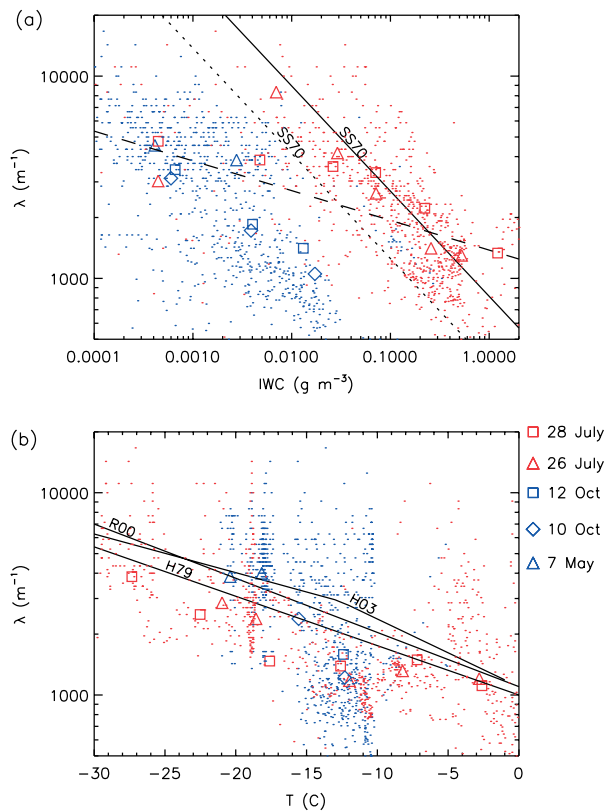


Figure 9. As in Figure 8, except for fitted λ as a function of (a) ice water content, IWC , and (b) temperature, T . Also shown are the relationships from Sekhon and Srivastava (1970; SS70, using an approach similar to Reisner *et al.* 1998), Ryan (2000; R00), Houze *et al.* (1979; H79), and Heymsfield (2003; H03). The dotted line shows the SS70 relationship with a correction to account for inconsistencies in the melted versus unmelted particle size. The dashed line indicates best-fit λ – IWC relationship (see text for details).

Overall, the shallow, low-level cases had much lower values of N_i and IWC than the deep cases, indicating substantial differences in ice generation and growth between these regimes. Large values of N_i were found throughout the depth of the cloud in the deep frontal cases. Within a given case for both the shallow and deep frontal systems, N_i had little correlation with temperature (height), even though an active aggregation process was indicated by observations of large aggregates (>5 mm) in four out of the five cases. Further, the presence of large aggregates near cloud top for the two shallow cases in which large aggregates were observed (10 and 12 October) suggests the role of turbulent updraughts and hence vertical mixing of ice particles. We hypothesize that primary and/or secondary ice particle formation in the lower part of the cloud layer (through rime-splintering, collisional breakup, or droplet freezing) may have helped to balance the depletion by aggregation to give relatively constant profiles of N_i through the depth of the clouds (in an average sense), although the available measurements are too limited to demonstrate this point conclusively.

Exponential PSDs were fitted to the observations and binned according to IWC and T . Values of N_0 were generally 2–10 times smaller for the shallow compared to the deep frontal cases. This was a result of much smaller values of N_i for the shallow cases, presumably due to differences in ice particle initiation between the shallow and deep cases. Values of snow $N_0 \sim 10^7 \text{ m}^{-4}$ specified in many bulk microphysics

schemes (e.g. Rutledge and Hobbs, 1983; Dudhia, 1989; Grabowski, 1998) are broadly consistent with the fitted N_0 for the deep cases but larger than in the shallow cases. The deep frontal cases exhibited a relationship between N_0 and T that was consistent with previous observational studies of midlatitude frontal cloud systems (Houze *et al.*, 1979; Field *et al.*, 2005) that have been used to parametrize snow N_0 as a function of T in some microphysics schemes (e.g. Hong *et al.*, 2004; Thompson *et al.*, 2004), while N_0 for the shallow cases were much smaller. There were no consistent differences in N_0 between the shallow and deep cases when partitioned by IWC . For the dataset as a whole, correlations between N_0 and IWC were higher than between N_0 and T . Thus, diagnosing N_0 as a function of IWC rather than T appears to be a more robust way to represent N_0 based on this dataset. The fitted λ for the shallow and deep cases were generally consistent with previous studies of lower-latitude cloud systems (SS70; Houze *et al.*, 1979; Ryan, 2000; Heymsfield, 2003).

Specification of N_0 is a major source of uncertainty in one-moment bulk microphysics schemes given its impact on several key microphysical processes. Previous modelling studies have shown that reducing N_0 for snow by about an order of magnitude from values of $\sim 10^7 \text{ m}^{-4}$ leads to more realistic simulations of shallow Arctic mixed-phase boundary-layer clouds (Morrison and Pinto, 2006; Solomon *et al.*, 2009). The present study has provided observational evidence for relatively low values of N_0 associated with these cloud systems relative to Arctic and midlatitude deep frontal systems. Two-moment bulk microphysics schemes allow N_0 to vary as a free parameter based on the predicted IWC and N_i , and hence could in principle capture variability of N_0 in shallow and deep regimes as well as variability as a function of local IWC based on the microphysical process rates. However, we emphasize that such schemes are dependent on the treatment of several highly uncertain microphysical processes that control the particle number concentration, in particular primary and secondary ice initiation. The ability of two-moment schemes to simulate the observed variability of N_0 and λ for these Arctic cases will be a subject of future work.

In general, observational data is limited in the Arctic compared with many other regions, especially when the focus is on particular cloud types or regimes. Thus, a limited number of case-studies (five) were available to develop the statistics presented herein. Generalization of these results will require analysis of additional cases from Arctic field experiments as these data become available. Ground and space-borne remote retrievals will also help to characterize snow microphysical characteristics in this region from a longer-term perspective.

Acknowledgements

Radar reflectivity data from Barrow and SHEBA were kindly provided by M. Shupe. We also thank M. Poellot for help in collecting the aircraft microphysical data, G. Zhang for his assistance in processing the MPACE data, and A. Fridlind, B. van Deidenhoven and A. Korolev for helpful discussions. This work was supported by US DOE ARM DE-FG02-08ER64574 (HM) and NASA InterDisciplinary Studies grant NNG04G171G (PZ). The work of GMM was supported by the Office of Science, US DOE ARM DE-FG02-02ER63337, DE-FG02-07ER64378

and DE-FG02-09ER64770. AB and AJH were supported by US DOE ARM DE-FG02-08ER64575. National Center for Atmospheric Research is sponsored by the National Science Foundation.

References

- Avramov A, Harrington JY. 2010. Influence of parameterized ice habit on simulated mixed phase Arctic clouds. *J. Geophys. Res.* **115**: D03205, DOI: 10.1029/2009JD012108.
- Brown PRA, Francis PN. 1995. Improved measurements of the ice water content in cirrus using a total-water probe. *J. Atmos. Oceanic Technol.* **12**: 410–414.
- Curry JA, Hobbs PV, King MD, Randall DA, Minnis P, Isaac GA, Pinto JO, Uttal T, Bucholtz A, Cripe DG, Gerber H, Fairall CW, Garrett TJ, Hudson J, Intrieri JM, Jakob C, Jensen T, Lawson P, Marcotte D, Nguyen L, Pilewskie P, Rangno A, Rogers DC, Strawbridge KB, Valero FPJ, Williams AG, Wylie D. 2000. FIRE Arctic Clouds Experiment. *Bull. Am. Meteorol. Soc.* **81**: 5–29.
- Dudhia J. 1989. Numerical study of convection observed during the Winter Monsoon Experiment using a mesoscale two-dimensional model. *J. Atmos. Sci.* **46**: 3077–3107.
- Field PR, Hogan RJ, Brown PRA, Illingworth AJ, Choulaton TW, Cotton RJ. 2005. Parametrization of ice-particle size distributions for mid-latitude stratiform cloud. *Q. J. R. Meteorol. Soc.* **131**: 1997–2017.
- Field PR, Heymsfield AJ, Bansemmer A. 2006. Shattering and particle interarrival times measured by optical array probes in ice clouds. *J. Atmos. Oceanic Technol.* **23**: 1357–1371.
- Fleishauer RP, Larson VE, Vonder Haar TH. 2002. Observed microphysical structure of midlevel, mixed-phase clouds. *J. Atmos. Sci.* **59**: 1779–1804.
- Fletcher NH. 1962. *The Physics of Rainclouds*. Cambridge University Press.
- Fridlind AM, Ackerman AS, McFarquhar GM, Zhang G, Poellot MR, DeMott PJ, Prenni AJ, Heymsfield AJ. 2007. Ice properties of single-layer stratocumulus during the Mixed-Phase Arctic Cloud Experiment. 2: Model results. *J. Geophys. Res.* **112**: D24202, DOI: 10.1029/2007JD008646.
- Fridlind AM, van Deidenhoven B, Ackerman AS, Avramov A, Morrison H, Zuidema P, Shupe MS. 2011. Entrainment limitations on heterogeneous ice formation: A FIRE-ACE/SHEBA case study of mixed-phase Arctic boundary layer clouds. *J. Atmos. Sci.* (submitted).
- Grabowski WW. 1998. Toward cloud resolving modeling of large-scale tropical circulations: A simple cloud microphysics parameterization. *J. Atmos. Sci.* **55**: 3283–3298.
- Gulpepe I, Isaac GA, Key J, Intrieri J, Starr DO'C, Strawbridge KB. 2004. Dynamical and microphysical characteristics of Arctic clouds using integrated observations collected over SHEBA during the April 1998 FIRE. ACE flights of the Canadian Convair. *Meteorol. Atmos. Phys.* **85**: 235–263.
- Gunn KLS, Marshall JS. 1958. The distribution with size of aggregate snowflakes. *J. Meteorol.* **15**: 452–461.
- Hallett J, Mossop SC. 1974. Production of secondary ice crystals during the riming process. *Nature* **249**: 26–28.
- Heymsfield AJ. 2003. Properties of tropical and midlatitude ice cloud particle ensembles. Part II: Applications for mesoscale and climate models. *J. Atmos. Sci.* **60**: 2592–2611.
- Heymsfield AJ, Parrish JL. 1978. A computational technique for increasing the effective sampling volume of the PMS two-dimensional particle size spectrometer. *J. Appl. Meteorol.* **17**: 1566–1572.
- Heymsfield AJ, Field PR, Bansemmer A. 2008. Exponential size distributions for snow. *J. Atmos. Sci.* **65**: 4017–4031.
- Hong S-Y, Dudhia J, Chen S-H. 2004. A revised approach to ice microphysical processes for the bulk parameterization of clouds and precipitation. *Mon. Weather Rev.* **132**: 103–120.
- Houze Jr RA, Hobbs PV, Herzegh PH, Parsons DB. 1979. Size distributions of precipitation particles in frontal clouds. *J. Atmos. Sci.* **36**: 156–162.
- Inoue J, Liu J, Pinto JO, Curry JA. 2006. Intercomparison of Arctic regional climate models: Modeling clouds and radiation for SHEBA in May 1998. *J. Climate* **19**: 4167–4178.
- Jiang H, Cotton WR, Pinto JO, Curry JA, Weissbluth MJ. 2000. Cloud resolving simulations of mixed-phase Arctic stratus observed during BASE: Sensitivity to concentration of ice crystals and large-scale heat and moisture advection. *J. Atmos. Sci.* **57**: 2105–2117.
- Klein SA, McCoy RB, Morrison H, Ackerman AS, Avramov A, de Boer G, Chen M, Cole JNS, Del Genio AD, Falk M, Foster MJ, Fridlind A, Golaz J-C, Hashino T, Harrington JY, Hoose C, Khairoutdinov MF, Larson VE, Liu X, Luo Y, McFarquhar GM, Menon S, Neggers RAJ, Park S, Poellot MR, Schmidt JM, Sednev I, Shipway BJ, Shupe MD, Spangenberg DA, Sud YC, Turner DD, Veron DE, von Salzen K, Walker GK, Wang Z, Wolf AB, Xie S, Xu K-M, Yang F, Zhang G. 2009. Intercomparison of model simulations of mixed-phase clouds observed during the ARM Mixed-Phase Arctic Cloud Experiment. I: Single-layer cloud. *Q. J. R. Meteorol. Soc.* **135**: 979–1002.
- Korolev AV, Emery EF, Strapp JW, Cober SG, Isaac GA, Wasey M, Marcotte D. 2010. Small ice particles in tropospheric clouds: Fact or artifact? Airborne Icing Instrumentation Evaluation Experiment. *Bull. Am. Meteorol. Soc.* (in press).
- Lawson RP, Zuidema P. 2009. Aircraft microphysical and surface-based radar observations of summertime Arctic clouds. *J. Atmos. Sci.* **66**: 3505–3529.
- Lawson RP, Baker BA, Schmitt CG, Jensen TL. 2001. An overview of microphysical properties of Arctic clouds observed in May and July 1998 during FIRE ACE. *J. Geophys. Res.* **106**: 14989–15014.
- Lin Y-L, Farley RD, Orville HD. 1983. Bulk parameterization of the snow field in a cloud model. *J. Clim. Appl. Meteorol.* **22**: 1065–1092.
- Locatelli JD, Hobbs PV. 1974. Fall speeds and masses of solid precipitating particles. *J. Geophys. Res.* **79**: 2185–2197.
- Luo Y, Xu K-M, Morrison H, McFarquhar GM, Wang Z, Zhang G. 2008. Multi-layer Arctic mixed-phase clouds simulated by a cloud-resolving model: Comparison with ARM observations and sensitivity experiments. *J. Geophys. Res.* **113**: D12208, DOI: 10.1029/2007JD009563.
- McFarquhar GM, Black RA. 2004. Observations of particle size and phase in tropical cyclones: Implications for mesoscale modeling of microphysical processes. *J. Atmos. Sci.* **61**: 422–439.
- McFarquhar GM, Zhang G, Poellot MR, Kok GL, McCoy R, Tooman T, Fridlind A, Heymsfield AJ. 2007. Ice properties of single-layer stratocumulus during the Mixed-Phase Arctic Cloud Experiment. Part I: Observations. *J. Geophys. Res.* **112**: D24201, DOI: 10.1029/2007JD008633.
- McFarquhar GM, Ghan S, Verlinde J, Korolev A, Strapp JW, Schmid B, Tomlinson JM, Wolde M, Brooks SD, Cziczo D, Dubey MK, Fan J, Flynn C, Gulpepe I, Hubbe J, Gilles MK, Laskin A, Lawson P, Leaitch WR, Liu P, Liu X, Lubin D, Mazzoleni C, Macdonald A-M, Moffet RC, Morrison H, Ovchinnikov M, Shupe MD, Turner DD, Xie S, Zelenyuk A, Bae K, Freer M, Glen A. 2010. Indirect and Semi-Direct Aerosol Campaign (ISDAC): The impact of Arctic aerosols on clouds. *Bull. Am. Meteorol. Soc.* **92**: 183–201.
- Magono C, Lee CW. 1966. Meteorological classification of natural snow crystals. *J. Fac. Sci. Hokkaido Univ. Ser. 7* **2**: 320–335.
- Mitchell DL, Zhang R, Pitter RL. 1990. Mass-dimensional relationships for ice particles and the influence of riming on snowfall rates. *J. Appl. Meteorol.* **29**: 153–163.
- Morrison H, Pinto JO. 2006. Intercomparison of bulk cloud microphysics schemes in mesoscale simulations of springtime Arctic mixed-phase stratiform clouds. *Mon. Weather Rev.* **134**: 1880–1900.
- Morrison H, Shupe MD, Curry JA. 2003. Modeling clouds observed at SHEBA using a bulk parameterization implemented into a single-column model. *J. Geophys. Res.* **108**: 4255, DOI: 10.1029/2002JD002229.
- Morrison H, Shupe MD, Pinto JO, Curry JA. 2005. Possible roles of ice nucleation mode and ice nuclei depletion in the extended lifetime of Arctic mixed-phase clouds. *Geophys. Res. Lett.* **32**: L18801, DOI: 10.1029/2005GL023614.
- Morrison H, McCoy RB, Klein SA, Xie S, Luo Y, Avramov A, Chen M, Cole JNS, Falk M, Foster MJ, Del Genio AD, Harrington JY, Hoose C, Khairoutdinov MF, Larson VE, Liu X, McFarquhar GM, Poellot MR, von Salzen K, Shipway BJ, Shupe MD, Sud YC, Turner DD, Veron DE, Walker GK, Wang Z, Wolf AB, Xu K-M, Yang F, Zhang G. 2009a. Intercomparison of model simulations of mixed-phase clouds observed during the ARM Mixed-Phase Arctic Cloud Experiment. II: Multilayer cloud. *Q. J. R. Meteorol. Soc.* **135**: 1003–1019.
- Morrison H, Thompson G, Tatarskii V. 2009b. Impact of cloud microphysics on the development of trailing stratiform precipitation in a simulated squall line: Comparison of one- and two-moment schemes. *Mon. Weather Rev.* **137**: 991–1007.
- Pinto JO. 1998. Autumnal mixed-phase cloudy boundary layers in the Arctic. *J. Atmos. Sci.* **55**: 2016–2038.
- Prenni AJ, Harrington JY, Tjernström M, DeMott PJ, Avramov A, Long CN, Kreidenweis SM, Olsson PQ, Verlinde J. 2007. Can ice-nucleating aerosols affect Arctic seasonal climate? *Bull. Am. Meteorol. Soc.* **88**: 541–550.
- Pruppacher HR, Klett JD. 1997. *Microphysics of Clouds and Precipitation*. Kluwer Academic.

- Reisner J, Rasmussen RM, Bruintjes RT. 1998. Explicit forecasting of supercooled liquid water in winter storms using the MM5 forecast model. *Q. J. R. Meteorol. Soc.* **124**: 1071–1107.
- Rutledge SA, Hobbs PV. 1983. The mesoscale and microscale structure and organization of clouds and precipitation in midlatitude cyclones. VIII: A model for the 'seeder-feeder' process in warm-frontal rainbands. *J. Atmos. Sci.* **40**: 1185–1206.
- Ryan BF. 2000. A bulk parameterization of the ice particle size distribution and the optical properties in ice clouds. *J. Atmos. Sci.* **57**: 1436–1451.
- Sekhon RS, Srivastava RC. 1970. Snow size spectra and radar reflectivity. *J. Atmos. Sci.* **27**: 299–307.
- Shupe MD, Matrosov SY, Uttal T. 2006. Arctic mixed-phase cloud properties derived from surface-based sensors at SHEBA. *J. Atmos. Sci.* **63**: 697–711.
- Solomon A, Morrison H, Persson POG, Shupe MD, Bao J-W. 2009. Investigation of microphysical parameterizations of ice and snow in Arctic clouds during M-PACE through model–observation comparisons. *Mon. Weather Rev.* **137**: 3110–3128.
- Strapp JW, Albers WF, Reuter A, Korolev AV, Maixner U, Rashke E, Vukovic Z. 2001. Laboratory measurements of the response of a PMS OAP-2DC. *J. Atmos. Oceanic Technol.* **18**: 1150–1170.
- Thompson G, Rasmussen RM, Manning K. 2004. Explicit forecasts of winter precipitation using an improved bulk microphysics scheme. Part I: Description and sensitivity analysis. *Mon. Weather Rev.* **132**: 519–542.
- Twohy CH, Strapp JW, Wendlich M. 2003. Performance of a counterflow virtual impactor in the NASA icing research tunnel. *J. Atmos. Oceanic Technol.* **20**: 781–790.
- Uttal T, Curry JA, McPhee MG, Perovich DK, Moritz RE, Maslanik JA, Guest PS, Stern HL, Moore JA, Turenne R, Heiberg A, Serreze MC, Wylie DP, Persson POG, Paulson CA, Halle C, Morison JH, Wheeler PA, Makshtas A, Welch H, Shupe MD, Intrieri JM, Stamnes K, Lindsey RW, Pinkel R, Pegau WS, Stanton TP, Grenfeld TC. 2002. Surface heat budget of the Arctic Ocean. *Bull. Am. Meteorol. Soc.* **83**: 255–275.
- Vardiman L. 1978. The generation of secondary ice particles in clouds by crystal–crystal collision. *J. Atmos. Sci.* **35**: 2168–2180.
- Verlinde J, Harrington JY, Yannuzzi VT, Avramov A, Greenberg S, Richardson SJ, Bahrman CP, McFarquhar GM, Zhang G, Johnson N, Poellot MR, Mather JH, Turner DD, Eloranta EW, Tobin DC, Holz R, Zak BD, Ivey MD, Prenni AJ, DeMott PJ, Daniel JS, Kok GL, Sassen K, Spangenberg D, Minnis P, Tooman TP, Shupe MD, Heymsfield AJ, Schofield R. 2007. The Mixed-Phase Arctic Cloud Experiment (M-PACE). *Bull. Am. Meteorol. Soc.* **88**: 205–221.
- York D, Evensen NM, López Martínez M, De Basabe Delgado J. 2004. Unified equations for the slope, intercept, and standard errors of the best fit straight line. *Am. J. Phys.* **72**: 367–375.
- Zuidema P, Baker B, Han Y, Intrieri JM, Key J, Lawson P, Matrosov S, Shupe MD, Stone R, Uttal T. 2005. An Arctic springtime mixed-phase cloudy boundary layer observed during SHEBA. *J. Atmos. Sci.* **62**: 160–176.